

Size Dependent Compressive Strength of FIB Machined Single Crystal Manganese Pillars

Halil Yılmaz^{1*}  Bulent Alkan²  Hasan Feyzi Budak³ 

¹ R. Mus Alparslan University, Department of Mechanical and Metal Technologies, Mus, Türkiye.

² R. Hittit University, Department of Metallurgy and Materials Engineering, Corum, Türkiye.

³ R. Ataturk University, East Anatolia High Technology Application and Research Center, Erzurum, Türkiye.

ABSTRACT

The deformation behavior of single crystals of manganese pillars generated by focused ion beam (FIB), with diameters ranging from $-1 \mu\text{m}$ to $-4.5 \mu\text{m}$, has been studied as a function of specimen size using micropillar compression at ambient temperature. The manganese pillars were machined from randomly chosen larger grains of polycrystalline metal. At ambient temperature, single crystals of manganese display chaotic slip planes emerging on the sample surface and brittle plastic deformation when the sample size is decreased to the micrometer scale. The manganese pillars reached very high flow stresses in the range of 4-5.6 GPa. The stress-strain curves of all tested manganese pillars demonstrated significant work hardening and smooth flow behavior, with strains up to 8-10%. After 10% strain, however, the flow stresses remained constant with no work hardening. As previously reported, the manganese pillars with undetermined crystal orientation demonstrated a less pronounced size effect (-0.14) by the size effect exponent of BCC pillars.

Keywords:

Focused ion beam; Manganese; Micropillar compression; Mechanical properties; Size effect

INTRODUCTION

Pure manganese is simply known as 'hard, brittle and silverly colored' metal, however why manganese is hard and is not entirely clear. The microcracks appearing during the phase transformation upon solidification are sometimes reported as one of the main causes of brittleness, since the varying displacements are accumulating during the multiphase transformation (1, 2).

Manganese resembles iron and is reasonably reactive that dissolves non-oxidizing acids. Additionally, it tends to rust when subjected to exposure to water. It has been widely used as the main additive in the production of steel and other alloys, thereby significantly enhancing their physical and mechanical properties. Manganese is important as an alloying element in ferrous and non-ferrous metal alloys to enhance corrosion resistance and strength. Furthermore, manganese dioxide is commonly employed as a cathode material in commercial batteries. (3, 4).

It is known that manganese undergoes isotropic phase transformation on cooling, beginning from δ to γ (at 1407 K), then to β (at 1368 K) and finally to α (at 1015

K). While δ to γ phases have body centered cubic (BCC) and face centered cubic (FCC) respectively. The β and α phases of manganese are known to have a complicated crystal structure with 20 and 58 atoms in the cubic cell, respectively. α -manganese has a complex crystal lattice of the A12-type based on the BCC structure with a lattice constant $\alpha \sim 8.9 \text{ \AA}$ (2, 5).

The use of advanced characterization techniques is one component in knowing the quality of such alloys or steels. However, evaluating small-volume materials differs from testing bulk materials. This is due to the occurrence of artifacts, such as in nanomechanical testing techniques. Mechanical properties and deformation behavior of small volume materials are critical in the effective design of small devices that must sustain stresses in service. (6, 7). Thus, mechanical testing of nanostructured materials fabricated by FIB machining allows the investigation of various sample geometries such as micropillar for compression (8, 9), dog-bone shape for tensile tests (10, 11), and cantilevers for bending (12, 13). Free-standing micropillar compression experiments are a promising method to examine the mechanical properties of single crystals of various materials with small

Article History:

Received: 2023/09/25

Accepted: 2024/01/22

Online: 2024/03/31

Correspondence to: Halil Yılmaz,
E-mail: halil.yilmaz@alparslan.edu.tr;
Phone: +90(436) 249 49 49 (2532)

This article has been checked for similarity.



This is an open access article under the CC-BY-NC licence

<http://creativecommons.org/licenses/by-nc/4.0/>

Cite as:

Yılmaz H, Alkan B, Budak HF. Size Dependent Compressive Strength of FIB Machined Single Crystal Manganese Pillars. Hittite Journal of Science and Engineering 2024;11(1):41-47. doi:10.17350/hjse19030000330

dimensions.

There are numerous reports published on compression experiments of metal nanopillars with diameters less than 5 μm . In all cases, the smaller the sample diameter, the higher the pillar/wire strength. This phenomenon is called size effect dependency. This dependence of strength on specimen size was first reported by Uchic et al. (8), whereby they used a FIB machining and nanomechanical testing device equipped with a flat-ended tip to investigate the in-situ mechanical properties of micron/submicron-sized nickel (Ni) pillars at room temperature (8, 14). They reported some shifts in the stress-strain plots as the pillar diameters varied and found an inverse relationship between yield stress and power of sample size. Consequently, this method has become more attractive and very popular for investigating the size effect dependence of various materials. Moreover, fundamental approaches were tried to understand the size effect dependence and deformation behaviors of small-sized materials and specially focused on different lattice types of materials such as FCC (8, 14-18), BCC (19-23), hexagonal close-packed (HCP) (24, 25), metallic glasses (26-28) and nanocrystalline materials (29). The FCC metal pillars under compression exhibited a universal power-law relation between pillar diameter and strength. The yield stress (σ_y) has an inverse relationship with the variable power of the sample size (d), with a universal empirical correlation:

$$\sigma_y = \sigma_0 + Ad^n \quad (1)$$

where, σ_0 represents a bulk strength, A represents a material constant, and n represents a size effect exponent. For several FCC lattices, the power-law exponents have been typically found to be in the range of -0.6 to -1.0. Dou and Derby compiled the size-dependent strength for several FCC nanowires/pillars (tested in compression) against sample diameter. This was proposed that a universal empirical relation of approximately $n = -0.67$, for equation 1, where $\sigma_0 = 0$ (30).

Equation 1 expresses a similar connection between compressive engineering stress and pillar/wire diameter for BCC metal pillars. However, samples of BCC metal tested under compression exhibit considerable variances in behavior with power-law exponents ranging from -0.15 to -0.8 (19, 21-23, 31-34). It is generally believed that the difference in the behavior between FCC and BCC metals is attributed to the different responses of dislocations in the different lattice structures. In FCC metal pillars, the dislocations are highly mobile, thereby showing similar mobility for edge and screw dislocations and need quite low thermal activation. However, in BCC structures, the coplanar core structure of a screw dislocation causes a higher lattice friction stress (Peierls) and lower mobility when than their edge counter-

parts, thus necessitating a higher level of thermal activation (19, 35, 36). Kishida et. al (37) examined the compression behavior of single crystal α -Mn micropillars with squared cross-sections ranging from 1 to 10.5 μm , against crystal orientation at the room temperature for the first time, and determined the deformation mechanism and critical resolved shear stress (CRSS). They discovered that single crystal manganese pillars deformed plastically due to dislocation motion and reached extremely high flow stresses in the 4.5-6 GPa range. Dislocations glide along [111] and [001] are pointed out to operate in Z-axis orientations near [001] and [111] respectively. Because of the wavy shape of slip planes induced by cross-slip, they were unable to identify the low-indexed planes.

Furthermore, the literature has extensive experimental research on the size-dependent mechanical characteristics of different single-crystal FCC and BCC metals. This suggests the evolution of the size effect, which could be instrumental in this regard. As a result, there is sufficient opportunity to improve understanding of the micromechanical properties of manganese pillars for the whole range of BCC metals size effects mentioned in the literature.

Thus, the purpose of this study is to investigate the size-dependent compressive strength and deformation behavior of single crystals manganese pillars against sample size at ambient temperature using micropillar samples with diameters ranging from ~ 1 to ~ 4.5 μm to deduce the size-dependent strength through evaluating flow stress values.

MATERIALS AND METHODS

Materials Used and Pillar Preparation

A cast polycrystalline pure Mn metal sheet (99.95%) having 2 mm thickness, denoted "as-received" material was provided from Goodfellow Cambridge Ltd. The samples were cut into small squares (10 mm \times 10 mm) and mounted in resin. The sample surface was gradually ground with SiC abrasive grinding papers (from P1200-grit to final grinding with P2000-grit; EU grade). This process was followed by polishing down to $\frac{1}{4}$ μm using diamond pastes in sequence. After that, further finishing was carried out using an active polishing suspension (OP-S) to remove the strain, induced by grinding and polishing operations. The specimen was extracted from the mount and placed onto scanning electron microscopy (SEM) stub for further characterization. Larger grains were selected to generate random orientation samples, which were subsequently processed using a FIB to fabricate micropillars of the desired dimensions.

All single crystal pillars with diameters ranging from ~ 1 μm to ~ 4.5 μm were prepared using FIB from randomly

selected grains of manganese. A free-standing Mn pillar was prepared using a Zeiss Gemini 2 Crossbeam 540 SEM-FIB (Carl Zeiss, Jena, Germany). This instrument was located at the East Anatolia High Technology Application and Research Center (DAYTAM)/Ataturk University. Accelerating voltages of 5 kV and 30 kV were utilized for imaging and machining (preparations), respectively. According to Volkert and Lilleodden's procedure, (38) the nano/micropillar machining process was performed in two stages. The methods and experimental conditions used to fabricate the micropillars have also been explained in detail in our earlier work (23). Briefly, the pillars were prepared using an inner and outer diameter ring pattern design. The radius of the inner and outer rings was set to approximately around 9 μm and 16 μm , respectively. The pillars of different heights were produced by utilizing a variety of dwell times. Depending on the required pillar height, a high flow of gallium (Ga^+) ions applied at the start of the FIB milled a hole around the pillar with a depth ranging from 18-32 μm . An individual Mn pillar was machined (at most $\frac{1}{4}$ of the grain size) from each selected grain in the Mn microstructure. The highest pillar fabricated was around 12.3 μm . Therefore, we chose a grain with around 50 μm to be sure that pillar does not contain any sub-grain or grain boundaries. The aspect ratio was set between 2.8 and 3.8, to avoid buckling deformation at higher pillar heights. This was accomplished by progressively decreasing the FIB current at various machining stages. From a milling point of view, the compression pillars with taper angles ranging from 3° to 5° were obtained. Based on the as-received conditions, the manganese metal only allows to machine/prepare a single pillar from an individual grain. Before the uniaxial compression experiments, the size of each pillar (all diameters and heights) was obtained using images collected with FIB (Zeiss Gemini Crossbeam 540, at 5kV).

Uniaxial Compression Experiments

Uniaxial compression tests on Mn pillars were carried out with the help of an Agilent Technologies Nano Indenter G200 micromechanical testing system (Agilent Technologies, Santa Clara, CA, USA) outfitted with a 15 μm flat punch tip. This instrument was located at Koç University Surface Science and Technology Center (KUYTAM). The compression tests were performed in displacement-rate control mode at a constant nominal displacement rate of 3 nm/s. Stress-strain graphs were created using the load-displacement data. As mentioned in our previous work, the size-dependent strength vs pillar diameter was displayed following standard compressive flow stress at 4% strain (23). This is because there is no uniform engineering strain value in the literature where micropillar compression experiments are reported, and the data are variably given in a 2.5-8% compressive strain range (22, 31, 39, 40).

RESULTS AND DISCUSSION

Microstructure

Several attempts have been made to examine the information about the microstructure of manganese metal sheet using electron backscatter diffraction (EBSD) analysis. It has been discovered that the surface of manganese metal cannot produce a single diffraction pattern. The crystal orientation of the grains could not be identified. Thus, larger grains were chosen at random to produce the manganese pillars. The Mn pillars of varying diameters were machined from randomly selected grains without regard for orientation. Therefore, due to the microstructure of manganese metal, it was impossible to fabricate multiple pillars in one grain. The SEM micrographs of the microstructure and FIB machined micropillars are depicted in Fig. 1 (a-c).

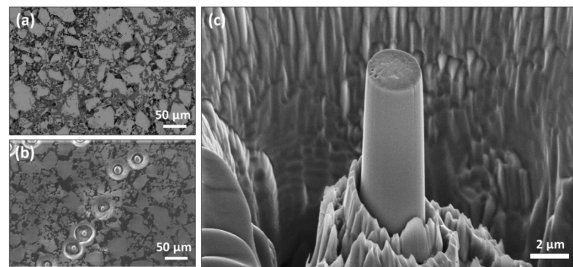


Figure 1. (a) SEM image of polycrystalline manganese metal surface, (b) A view of some micropillars prepared by FIB on the surface of Mn metal, and (c) A representative SEM image of 2.6 μm Mn micropillar in diameter. The image was taken at 54° tilt from the top view.

Crystallographic Slip for Manganese Pillars

Fig. 2 shows typical SEM micrographs of manganese pillars varying in diameter from ~1 μm to ~4.5 μm . These Mn pillars were machined from randomly picked grains and compressed. It should be highlighted that without knowing the grain orientation, we couldn't tell which slip planes were engaged during compression from the chaotic slip bands. There was no substantial variation in deformation behavior between deformed manganese pillars with undetermined orientation. In the top right SEM image in Fig. 2, the clear slip traces are more apparent compared to other SEM images since there is no load controlling option in testing instrument. The testing instrument has only displacement-rate control mode. We were not able to control the load applied. Thus, the applied load was too high for some pillars to identify the slip traces. Also, the orientations of the grains are uncertain, the angle between the loading direction and the normal of the slip plane could not be calculated. In this study, we aimed to investigate the effect of pillar diameter on strength rather than aspect ratio or the effect of length. Researchers tend to give more attention to studying the effect of pillar diameter on the mechanical properties of micro- or nanoscale materials due to its significant influ-

ence, ease of precise control during fabrication (FIB and lithography), and its pronounced size-dependent behaviors in small-scale materials. Variations in pillar diameter often lead to more pronounced size effects in mechanical properties due to high surface-to-volume ratio, which becomes critical at smaller dimensions. Changes in diameter can create significant differences in stress distributions and deformation mechanisms compared to heights variation. For example, changes in diameter can influence the density of defects, stress concentrations, and surface effects (dislocation image force, dislocation starvation mechanism etc.) more prominently than variations in height. (41, 42)

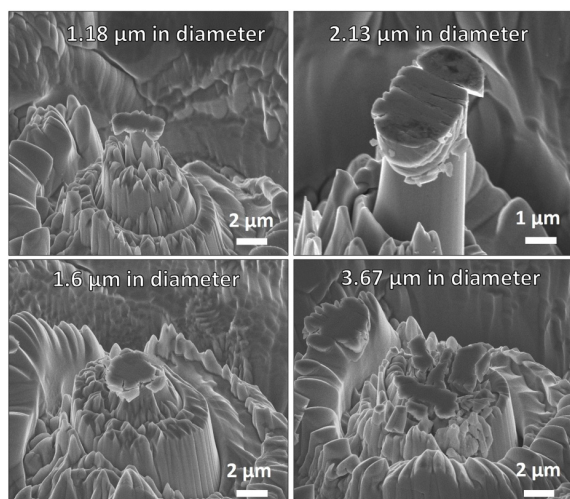


Figure 2. post deformation SEM images of Mn pillars with various diameters. On the surface of the pillars, a chaotic and brittle slip behavior was observed. SEM images were captured and adjusted at 36° from the top view.

Stress-Strain Curves and Size Effect Dependency

Fig. 3 indicates a representative engineering stress-strain plot for randomly selected orientations of manganese pillars with various diameters. This curve clearly showed the influence of sample size on the pillar strength. Since then, the stress has increased as the pillar size has reduced. At 4% strain, the flow stress reached 5.61 GPa for manganese pillars with a diameter of 1182 nm. Due to early plasticity, the yield stress at 0.2% strain is quite difficult to apply in these pillar experiments. Therefore, we have chosen a fixed strain (4%) in our pillar study. At 4% strain, the stress of the largest manganese pillar (4460 nm) was 4.53 GPa. The stress-strain plot for manganese metal shows a period of indistinct yield onset followed by strain hardening up to 10% strain. In general, the stress-strain curves of all tested manganese pillars showed high work hardening and smooth flow behavior, typically with strains up to 8-10%. However, the flow stresses remained constant without work hardening after 10% strain. No significant difference was found in the stress-strain be-

havior of all Mn pillars tested in unknown orientations. When compared to other BCC metallic pillars examined in the literature, the Mn pillars demonstrated considerably greater engineering stresses at 4% strain for a given diameter. The Mn pillars showed relatively higher engineering stresses for a specific diameter compared to other BCC metallic pillars tested in the literature (19, 22, 23, 34, 40). Our stress-strain results agree with previously reported only single study on Mn pillars, confirming that higher stresses (ranging between 4-6 GPa) are reached for all orientations. The steepness in linear region in stress-strain behavior of Mn pillars was also observed similar in previously reported study on Mn pillars (37).

A possible explanation for the higher strength could be related to the arbitrary chosen orientations leading to non-uniform slip behavior and the unknown Schmid factor causing higher stress values than other metallic pillars reported in the literature. The local dislocation density in the Mn sample was not measured. However, the metal specimen displayed homogeneous and isotropic grain shapes. Thus, we conclude that the local dislocation densities were not too high to strongly influence our experiments and arguments.

The effect of pillar size on strain hardening rate (SHR) lowers as pillar diameter increases. The SHR data was derived as the mean gradient of the stress-strain curve between 4% and 10% strain, which is consistent with earlier compression investigations (see Fig. 4). (19, 21, 23, 40, 43). The SHR data was precisely identified through data extraction using data reader function in the Origin Lab software. Although some scatter was observed in the SHR data, indications of a size effect were discernible. The tests conducted on a larger number of pillars will reduce the observed data scatter. Our analysis did not identify error bars or ranges in the SHR data. Experiments using Mn pillars with known orientation must be repeated to determine why the flow stress and SHR were too high. Further research into the size-dependent mechanical behaviors of Mn pillars with known orientation is required to offer a statistically confirmed stress-strain curves to detect the active slip system and a more precise size effect exponent. Maintaining consistent fabrication processes for pillar fabrication, specifically in terms of uniform diameters, alongside constant testing parameters, is anticipated to comparable stress-strain, SHR data, and size effect exponents. Repetition of these experiments is expected to yield results consistent with this expectation.

Fig. 5 depicts the stress at 4% strain as a logarithmic curve vs pillar diameter. Linear interpolation was used to get the size effect exponent for the Mn pillars. As observed with the randomly oriented Mn pillars, there is a less apparent size effect, with flow stress increasing as pillar size decreases. The size effect exponent for Mn pillars was found

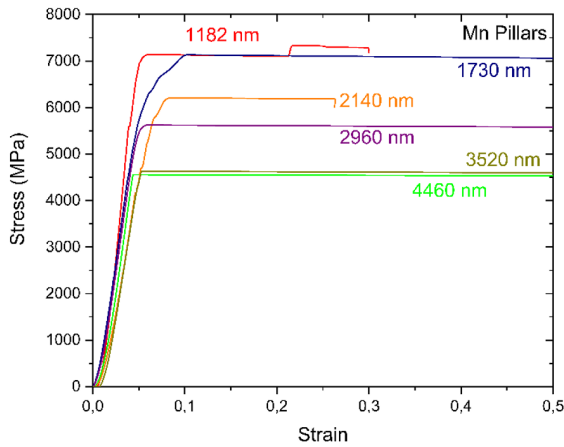


Figure 3. Typical stress-strain curves for compression tests conducted on Mn pillars

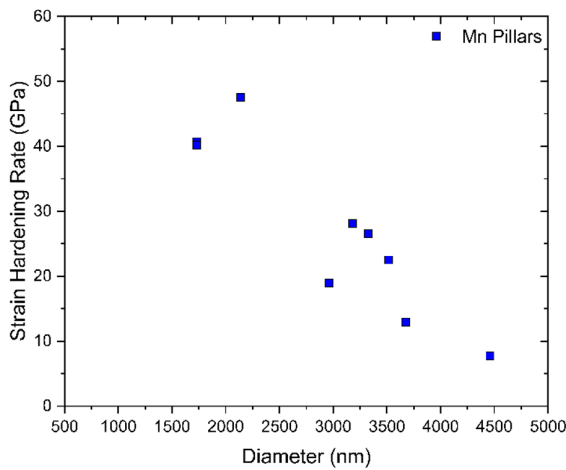


Figure 4. The relationship between strain hardening rate and manganese pillar diameters under compression.

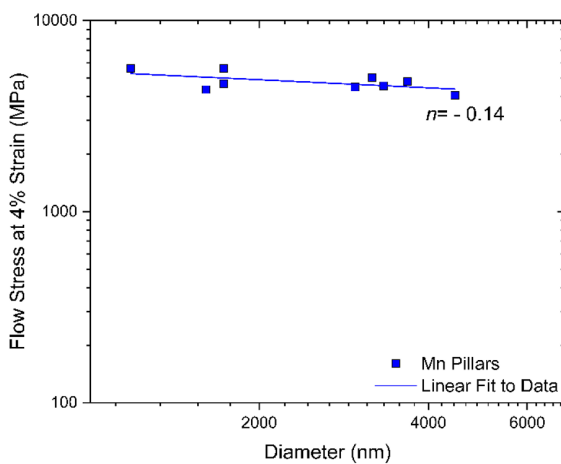


Figure 5. Logarithmic plot of engineering stress (at 4% strain) vs pillar diameter for compression tested Mn micropillars. The blue line represents a linear fit to the Mn data.

to be -0.14. According to the literature, the size exponents for BCC metals range between -0.1 and -0.8. The power law exponent of the Mn pillars agrees with prior research

on the BCC pillars. (19, 32, 34, 44). Kishida and colleagues (37) investigated how single crystal α -Mn micropillars with diameters ranging from 1 to 10.5 μm responded to compression testing concerning their crystal orientation. However, there does not appear to be a significant effect on yield stress due to sample size variations across the orientations studied. There is always uncertainty in determining the precise orientation of each pillar, which might cause variation in size effect data. Table 1 presents data from various reports on micropillars tests on several BCC metals.

Table 1. Data for the stress-size exponent, n , micro compression data with BCC metal pillars tested at ambient temperature.

| Material | Pillar Orientation | Active Slip System | n | Plastic Strain | Ref. |
|----------|---------------------|--------------------|-------|----------------|-----------|
| Mn | Random Orientations | Unknown | -0.14 | 4% | This work |
| Fe | [001] | {101}<111> | -0.58 | 4% | (23) |
| Fe | [110] | {101}<111> | -0.61 | 4% | (45) |
| Fe | [123] | {101}<111> | -0.63 | 4% | (45) |
| V | [001] | {101}<111> | -0.56 | 4% | (23) |
| Nb | [001] | {101}<111> | -0.58 | 4% | (23) |
| Ta | [001] | {101}<111> | -0.4 | 4% | (44) |
| W | [111] | {101}<111> | -0.23 | 4% | (44) |
| Mo | [111] | {101}<111> | -0.37 | 4% | (44) |

CONCLUSION

Single crystal manganese micropillars with randomly chosen crystallographic orientations were fabricated by FIB from a polycrystalline sample (varying in diameter from 1000-4500 nm) and deformed to measure their stress at 4% strain and deformation behavior. The following are the final thoughts:

- As the diameter of the manganese pillars decreased, the deformation behavior stayed constant and followed the same pattern. We were unable to discover an active slip mechanism due to the randomly picked grains.
- The stress-strain curves show that the flow stresses were higher compared to other BCC metals at specific diameters in the literature.
- The manganese pillars exhibited a less pronounced size effect, i.e. strength increased as pillar size decreased, resulting in a size effect exponent (n) of -0.14.
- Furthermore, the manganese pillars demonstrated strain hardening up to 10%, which increased as the pillar diameter decreased.

ACKNOWLEDGEMENT

This work was supported by Mus Alparslan University Scientific Research Project (BAP) of Mus Alparslan University under a project number of BAP-20-TBMY-4901-02.

We would like to thank the Eastern Anatolia High Technology Application and Research Center (DAYTAM) for access to the SEM and FIB.

CONFLICT OF INTEREST

Authors approve that to the best of their knowledge, there is not any conflict of interest or common interest with an institution/organization or a person that may affect the review process of the paper.

AUTHOR CONTRIBUTION

Halil Yilmaz: Conceptualization, Methodology, Investigation, Writing- original draft

Bulent Alkan: Investigation, Writing-review

Hasan Feyzi Budak: Methodology, Writing- review and editing

REFERENCES

1. Matricardi LR, Downing J. Manganese and manganese alloys. Kirk-Othmer Encyclopedia of Chemical Technology. 2000.
2. Sully A, Senderoff S. Manganese, Metallurgy of the Rarer Metals, Number 3. J Electrochem Soc. 1955;102(10):255Ca.
3. Verhoeven JD. Steel metallurgy for the non-metallurgist: ASM International; 2007. 220 p.
4. Martha S, Markovsky B, Grinblat J, Gofer Y, Haik O, Zinigrad E, et al. LiMnPO₄ as an advanced cathode material for rechargeable lithium batteries. J Electrochem Soc. 2009;156(7):A541.
5. Meaden GT. The general physical properties of manganese metal. Metallurgical Reviews. 1968;13(1):97-114.
6. Stelmashenko N, Walls M, Brown L, Milman YV. Microindentations on W and Mo oriented single crystals: an STM study. Acta Mater. 1993;41(10):2855-65.
7. Zhu T, Bushby A, Dunstan D. Materials mechanical size effects: a review. Mater Sci Technol. 2008;23(4):193-209.
8. Uchic MD, Dimiduk DM, Florando JN, Nix WD. Sample dimensions influence strength and crystal plasticity. Science. 2004;305(5686):986-9.
9. Greer JR, Oliver WC, Nix WD. Size dependence of mechanical properties of gold at the micron scale in the absence of strain gradients. Acta Mater. 2005;53(6):1821-30.
10. Kim J-Y, Greer JR. Tensile and compressive behavior of gold and molybdenum single crystals at the nano-scale. Acta Mater. 2009;57(17):5245-53.
11. Kiener D, Grosinger W, Dehm G, Pippan R. A further step towards an understanding of size-dependent crystal plasticity: In situ tension experiments of miniaturized single-crystal copper samples. Acta Mater. 2008;56(3):580-92.
12. Chen C, Pei Y, De Hosson JTM. Effects of size on the mechanical response of metallic glasses investigated through in situ TEM bending and compression experiments. Acta Mater. 2010;58(1):189-200.
13. Iqbal F, Ast J, Göken M, Durst K. In situ micro-cantilever tests to study fracture properties of NiAl single crystals. Acta Mater. 2012;60(3):1193-200.
14. Dimiduk D, Uchic M, Parthasarathy T. Size-affected single-slip behavior of pure nickel microcrystals. Acta Mater. 2005;53(15):4065-77.
15. Frick C, Clark B, Orso S, Schneider A, Arzt E. Size effect on strength and strain hardening of small-scale [111] nickel compression pillars. Mater Sci Eng A. 2008;489(1):319-29.
16. Ng K, Ngan A. Stochastic nature of plasticity of aluminum micropillars. Acta Mater. 2008;56(8):1712-20.
17. Kiener D, Motz C, Dehm G. Micro-compression testing: A critical discussion of experimental constraints. Mater Sci Eng A. 2009;505(1):79-87.
18. Kiener D, Motz C, Dehm G. Dislocation-induced crystal rotations in micro-compressed single crystal copper columns. J Mater Sci. 2008;43(7):2503-6.
19. Schneider AS, Kaufmann D, Clark BG, Frick CP, Gruber PA, Mönig R, et al. Correlation between critical temperature and strength of Small-Scale bcc pillars. Phys Rev Lett. 2009;103(10):105501.
20. Rogne BRS, Thaulow C. Effect of crystal orientation on the strengthening of iron micro pillars. Mater Sci Eng A. 2015;621:133-42.
21. Kaufmann D, Mönig R, Volkert C, Kraft O. Size dependent mechanical behaviour of tantalum. Int J Plast. 2011;27(3):470-8.
22. Kim J-Y, Jang D, Greer JR. Tensile and compressive behavior of tungsten, molybdenum, tantalum and niobium at the nanoscale. Acta Mater. 2010;58(7):2355-63.
23. Yilmaz H, Williams CJ, Risan J, Derby B. The size dependent strength of Fe, Nb and V micropillars at room and low temperature. Mater. 2019;7:100424.
24. Shan Z. In situ TEM investigation of the mechanical behavior of micronanoscaled metal pillars. JOM. 2012;64(10):1229-34.
25. Prasad KE, Rajesh K, Ramamurty U. Micropillar and macropillar compression responses of magnesium single crystals oriented for single slip or extension twinning. Acta Mater. 2014;65:316-25.
26. Mridha S, Arora HS, Lefebvre J, Bhowmick S, Mukherjee S. High temperature in situ compression of thermoplastically formed nanoscale metallic glass. JOM. 2017;69(1):39-44.
27. Shan Z, Li J, Cheng Y, Minor A, Asif SS, Warren O, et al. Plastic flow and failure resistance of metallic glass: Insight from in situ compression of nanopillars. Phys Rev B. 2008;77(15):155419.
28. Dubach A, Raghavan R, Löffler JF, Michler J, Ramamurty U. Micropillar compression studies on a bulk metallic glass in different structural states. Scripta Mater. 2009;60(7):567-70.
29. Cheng GM, Jian WW, Xu WZ, Yuan H, Millet PC, Zhu YT. Grain size effect on deformation mechanisms of nanocrystalline bcc metals. Mater Res Lett. 2012;1(1):26-31.
30. Dou R, Derby B. A universal scaling law for the strength of metal micropillars and nanowires. Scripta Mater. 2009;61(5):524-7.
31. Rogne B, Thaulow C. Strengthening mechanisms of iron micropillars. Philos Mag. 2015;95(16-18):1814-28.
32. Huang R, Li Q-J, Wang Z-J, Huang L, Li J, Ma E, et al. Flow stress in submicron BCC iron single crystals: sample-size-dependent strain-rate sensitivity and rate-dependent size strengthening. Mater Res Lett. 2015;3(3):121-7.
33. Han SM, Feng G, Jung JY, Jung HJ, Groves JR, Nix WD, et al. Critical-temperature/Peierls-stress dependent size effects in body centered cubic nanopillars. Appl Phys Lett. 2013;102(4):041910.
34. Lee S-W, Cheng Y, Ryu I, Greer J. Cold-temperature deformation of nano-sized tungsten and niobium as revealed by in-situ nano-mechanical experiments. Science China Technological Sciences. 2014;57(4):652-62.
35. Seeger A. Peierls barriers, kinks, and flow stress: Recent progress: Dedicated to Professor Dr. Haël Mughrabi on the occasion of his 65th birthday. Z Metallk. 2002;93(8):760-77.

36. Christian J. Some surprising features of the plastic deformation of body-centered cubic metals and alloys. *Metall Trans A*. 1983;14(7):1237-56.
37. Kishida K, Suzuki H, Okutani M, Inui H. Room-temperature plastic deformation of single crystals of α -manganese-hard and brittle metallic element. *Int J Plast*. 2023;160:103510.
38. Volkert CA, Lilleodden ET. Size effects in the deformation of sub-micron Au columns. *Philos Mag*. 2006;86(33-35):5567-79.
39. Schneider A, Clark B, Frick C, Gruber P, Arzt E. Effect of orientation and loading rate on compression behavior of small-scale Mo pillars. *Mater Sci Eng A*. 2009;508(1):241-6.
40. Torrents Abad O, Wheeler JM, Michler J, Schneider AS, Arzt E. Temperature-dependent size effects on the strength of Ta and W micropillars. *Acta Mater*. 2016;103:483-94.
41. Greer JR, Nix WD. Nanoscale gold pillars strengthened through dislocation starvation. *Phys Rev B*. 2006;73(24):245410.
42. Greer JR, De Hosson JTM. Plasticity in small-sized metallic systems: Intrinsic versus extrinsic size effect. *Prog Mater Sci*. 2011;56(6):654-724.
43. Kim J-Y, Greer JR. Size-dependent mechanical properties of molybdenum nanopillars. *Appl Phys Lett*. 2008;93(10):101916.
44. Yilmaz H. Mechanical properties of body-centred cubic nanopillars [PhD Thesis]: University of Manchester (Manchester, UK); 2018.
45. Yilmaz H, Williams CJ, Derby B. Size effects on strength and plasticity of ferrite and austenite pillars in a duplex stainless steel. *Mater Sci Eng A*. 2020;793:139883.